Proceedings

Precision Measuring Instrument and Method of Fertilizer Shape Characteristics Based on Binocular Vision †

Hongjian Zhang [1], Hao Jiang [2], Shuangxi Liu [1,2], Xuemei Liu [1], Chunbao Xu [1] and Jinxing Wang [1,3,*]

[1] College of Mechanical and Electronic Engineering, Shandong Agricultural University, Taian 271018, China; zhanghongji_an@163.com(H.Z.) ; 2019110098@sadu.edu.cn(H.J.) ; shuangxiliu168@163.com(S.L.) ; 2019120072@sadu.edu.cn(X.L.) ;2019120082@sadu.edu.cn(C.X.) ; jinxingw@163.com(J.W.)
[2] Shandong Provincial Key Laboratory of Horticultural Machinery and Equipment, Taian 271018, China
[3] Shandong Provincial Engineering Laboratory of Agricultural Equipment Intelligence, Taian 271018, China
* Correspondence: jinxingw@163.com

† Presented at 1st International Electronic Conference on Applied Sciences, 10–30 November 2020; Available online: https://asec2020.sciforum.net/.

Published: 10 November 2020

Abstract: Aiming at the low precision of manual measurement which also impose heavy workload burdern, as well as the high cost and complex operation of high-precision measuring instruments, a precision measuring instrument and method of fertilizer shape characteristics are proposed. In this method, the fertilizer shape characteristics are calculated by image acquisition, gray and gamma correction, and edge detection. Firstly, the measuring instrument works in an intermittent collection mode, which can acquire the top and side images of fertilizer at the same time. Secondly, gamma correction is performed on the top and side grayscale images to improve the image contrast, after the fertilizer image collection is completed. Finally, the edge detection algorithm based on the orientation gradient is proposed to extract the top and side contour images of the fertilizer accurately, and the shape characteristics are calculated from the contour images. The shape characteristics of the compound fertilizer, the organic fertilizer, and the biological fertilizer are measured by using the three-dimensional scanning method and the measuring method proposed in this paper. The significant difference between the two methods is compared by the Grubbs test, F test, and t test. The results show that there is no significant difference between the two measuring methods of fertilizer shape characteristics. This precision measuring instrument as well as its measuring method proposed in this paper can measure the fertilizer shape characteristics quickly and accurately, which can lay a solid foundation for fertilizer production and quality inspection.

Keywords: fertilizer; shape characteristics; measuring instrument; measuring method; binocular vision

1. Introduction

Particle shape characteristics are a classic and increasingly popular research topic in many disciplines [1-5]. The particle shape characteristics affect the mechanical and flow behavior of the material. For example, the sand tends to have a high angle of shear strength [6-7], the contact stress concentration [8-9], resistance to flow and anti-liquefaction resistance [10-11]. In addition, particle shape characteristics also affect the interaction of particles with fluids and air, such as drag coefficients and mineral floatability [12-13]. Therefore, particle shape is an important charateristics for predicting and controlling the engineering properties of particle materials.

Fertilizer is one of the most important agricultural particles, and its shape characteristics affect the appearance quality, strength, fluidity, and the effect of machine fertilization, which is of great significance to the design and research of agricultural machinery [14-15]. Kan, Su, and Tang [16] demonstrated that the higher the sphericity of fertilizer is, the higher the strength of fertilizer is, and the more difficult the fertilizer is to be deformed and broken. Silverberg, Lehr, and Hoffmeister [17] investigated that the shape characteristics and the pore structure formed by the accumulation of fertilizer affect the salt ions diffusion, so as to affect the performance of fertilizer. Basu and Kumar [18] found that fertilizer granularity affects the nutrient release time of fertilizer.

Fertilizer is an irregular shape particle, so it is difficult to measure the shape characteristics accurately manually. With the rapid development of computer and software technology, it is possible to measure the particle shape with the help of computer technology. Fernlund [19] measured the axial length of the long axis, the middle axis, and the short axis of the coarse aggregate by the image analysis method. The results show that the measurement results of this method have a good correlation with the measurement results of the Danish box. Zhang, Huang, and Zhao [20] measured the length, width, height, and particle shape index of the basalt and limestone by the digital image processing technology. Mora and Kwan [21] measured the sphericity and concave convex ratio of coarse aggregate by the digital image processing technology. Liu, Xiang, Budhu, and Cui [22] calculated and quantified the shape characteristics of sand particles by digital image processing. Zhang, Ye, Chen, and Li [23] measured and evaluated the shape characteristics of gravel particles by the digital image processing technology. Xiao, Yang, Chen, and Gao [24] used the digital image processing technology to calculate the particle shape and angular characteristic parameters of the aggregate.

Based on the above researches, it is found that the fertilizer shape characteristics affect fertilizer quality and performance. At present, there is no special particle shape measuring instrument for fertilizer. The manual measurement has high work intensity and low accuracy. The existing non-contact measuring instruments are mainly monocular, and they are mostly used to measure the aggregate and other particles. To measure the fertilizer shape characteristics accurately and quickly, a precision measuring instrument of fertilizer shape characteristics based on binocular vision as well as its measuring method are proposed in this paper. The non-contact measuring instrument is used to collect fertilizer images, and the fertilizer shape characteristics are extracted by the digital image processing technology.

2. Materials and Methods

2.1. Description Method of Fertilizer Shape Characteristics

2.1.1. Triaxial Characteristics

The macro profile of particles is usually represented by three mutually perpendicular axes, namely the long axis, the middle axis, and the short axis, which are equivalent to the length, width, and thickness of the particle. In a natural and stable state, the length refers to the maximum size of the particle in the plane projection graph, the width refers to the maximum size perpendicular to the length direction, and the thickness refers to the linear size perpendicular to the length and width direction. The relationship between the three axes of particles can be expressed by the equiaxed ratio and the flake ratio [25]:

$$K = b/a \tag{1}$$

$$\lambda = c/b \tag{2}$$

Where, k is the particle equiaxed ratio; λ is the particle flake ratio; a is the particle length, mm; b is the particle width, mm; c is the particle thickness, mm.

2.1.2. Roundness

Roundness (σ) reflects the sharpness of the particle edges and corners. Kuo and Freeman[26] define the particle roundness σ as follows:

$$\sigma = 4\pi A/L^2 \tag{3}$$

Where, L is the perimeter of the particle projection contour, mm; A is the projection area of the particle, mm^2.

2.1.3. Sphericity

Sphericity (φ) reflects how close the particle is to a sphere. Waddell defines the particle sphericity φ[27] as follows:

$$\varphi = \sqrt[3]{v/v_s} \tag{4}$$

According to Waddell's definition of the particle sphericity, Krumbein equates the particle as an ellipsoid[28], so the particle equivalent volume v is:

$$v = (\pi/6)abc \tag{5}$$

Substitute into the formula (4) to obtain the formula for calculating the particle sphericity:

$$\varphi = \sqrt[3]{v/v_s} = \sqrt[3]{(\pi/6)abc/(\pi/6)a^3} = \sqrt[3]{bc/a^2} \tag{6}$$

Where, v is the equivalent volume of the particle, mm^3; v_s is the volume of the smallest sphere circumscribed by the particle (sphere with a diameter as the diameter), mm^3.

2.1.4. Granularity

Granularity (d) is used to indicate the size of the particle, which can be expressed as the single size of a particle or the average particle size of a particle group. The granularity (d) of a single spheroid is as follows[29]:

$$d = \sqrt[3]{6v/\pi} = \sqrt[3]{abc} \tag{7}$$

Where, d is the particle granularity, mm.

2.2. Measuring Instrument of Fertilizer Shape Characteristics

The structure of the measuring instrument based on the binocular vision is shown in Figure 1. It is mainly composed of the base, the objective stage, the stepper motor, the top camera, the top lens, the side camera, the side lens, the upper computer, and the lower microcomputer. The main technical parameters of the instrument are shown in Table 1. The instrument adopts the intermittent static collection mode to collect the top and side images of single fertilizer at the same time. The objective stage is engraved with a cross calibration, and the fertilizer to be tested is placed at the center of the cross calibration. The objective stage is connected to the stepper motor through a semicircle key. The lower microcomputer controls the rotation of the stepping motor to achieve the rotation of the fertilizer. After the stepper motor turns the set angle, it stops rotating. The lower microcomputer sends the rotation completion command to the upper computer through the serial port. The upper computer controls the top and side cameras to collect the images of the fertilizer to be tested. After the image acquisition is completed, the upper computer sends the image acquisition completion command to the lower microcomputer through the serial port, and the lower microcomputer controls the stepping motor to rotate again. Repeat this process until the top and side images achieve the target number. The acquisition process is shown in Figure 1. After the top and side images of single fertilizer are all collected, the computer analyzes and processes the images respectively to obtain the fertilizer shape characteristics.

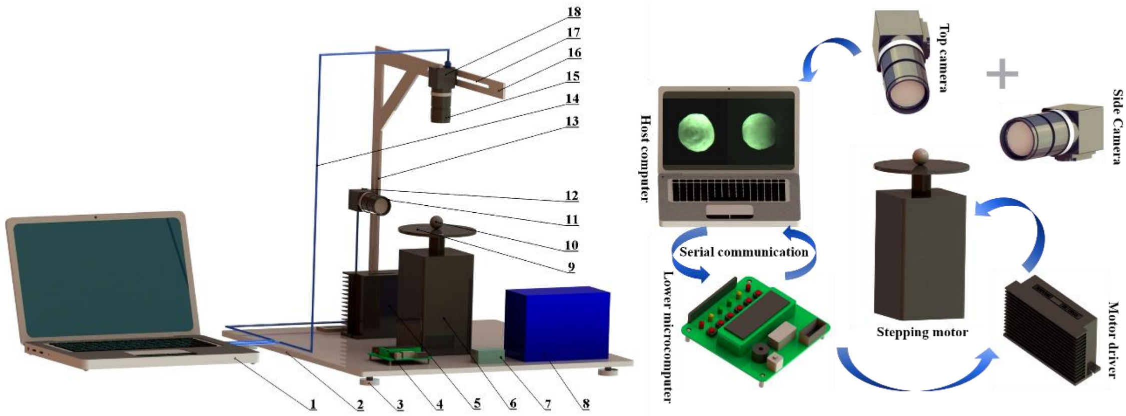

.

Figure 1. Structure of instrument and fertilizer collection process: (1)Upper computer; (2)Base; (3)Adjusting foot; (4)Lower microcomputer; (5)Driver; (6)Stepping motor; (7)Power conversion module; (8)Power; (9)Loading platform; (10)Fertilizer to be tested; (11)Side lens; (12)Side camera; (13)Side notch; (14)Data transmission line; (15)Top lens; (16)Camera adjusting frame; (17)Top notch; (18)Top camera.

Table 1. Main technical parameters.

Parameters	Numerical value
Overall dimensions (length × width × height)/(mm×mm×mm)	450×450×435
Loading platform size (radius)/mm	115
Working voltage/ V	24
Stepper motor speed/ r·min^{-1}	21
Single particle fertilizer collection time/ s	28
Fertilizer sampling interval/ s	16
Working distance of top camera/ mm	180
Side camera working distance/ mm	180

2.3. Measuring Method of Fertilizer Shape Characteristics

2.3.1. Length Calibration

To establish the relationship between the actual size of the fertilizer and the pixels, the image information of the calibration target (10mm×10mm black square) is collected, and the grayscale and binarization process is performed. The process is shown in Figure 2. In the threshold image, the target area is black, and the threshold value is 0. The threshold image is traversed by pointer scanning, and the number of rows of all pixels that meet the defined threshold is counted N_0=550. According to formula (8), the actual length represented by a single pixel (L_0) is 0.018mm.

$$L_0 = 10/ N_0 \tag{8}$$

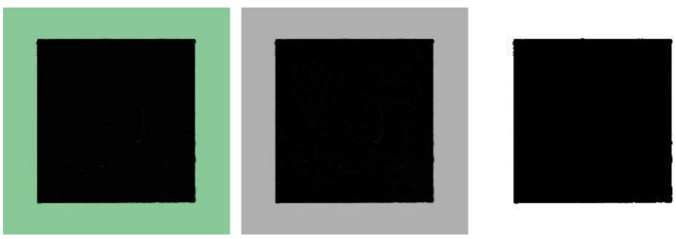

(a) (b) (c)

Figure 2. Length calibration: (**a**) Original image; (**b**) Grayscale image; (**c**) Threshold image.

2.3.2. Collection and Preprocessing of Fertilizer Images

Firstly, we should place a single fertilizer at the center of the cross calibration, and adjust the positions of the cameras to ensure that the fertilizer is completely imaged in the two cameras. Secondly, we should adjust the light intensity and focal length according to the imaging state of the fertilizer in the top and side cameras to ensure that the top and side images are clear and stable. Finally, to better get the whole side profile of the fertilizer, we should collect different sides profiles of the fertiliezer in different angles. Therefore, we controll the stepper motor to rotate 9° for a step and the stepper motor will rotate 20 steps in one time, and the top and side cameras respectively collect the top and side images of the fertilizer [30]. In the process of rotation, the contour of the top image is all the same, therefore, the top image is collected once, while the side image needs to be collected many times. After the collection, a total of 1 top image and 20 side images are obtained. To describe the fertilizer details more clearly, we crop the area containing the complete fertilizer image to display in the paper. The top image and some side images of the fertilizer are shown in Figure 3.

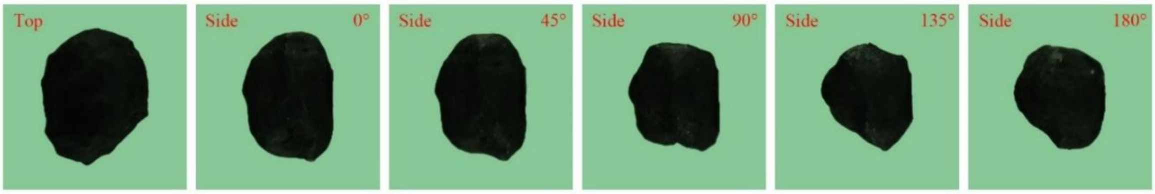

Figure 3. Original images of fertilizer top and side.

Gamma correction is a non-linear operation on the gray value of the input image, which makes the gray value of the output image exponentially related to the gray value of the input image. It is usually used for smoothing the extended dark details. In order to improve the extraction accuracy of fertilizer contour, the collected fertilizer image is processed with greyscale first, and then the gray image is corrected with gamma according to formula (9). The correction effect is shown in Figure 4.

$$Y(x,y) = I(x,y)^{\gamma} \tag{9}$$

Where, $I(x, y)$ is the gray image; $Y(x, y)$ is the corrected image; (x, y) is the pixel coordinates; γ is 0.5.

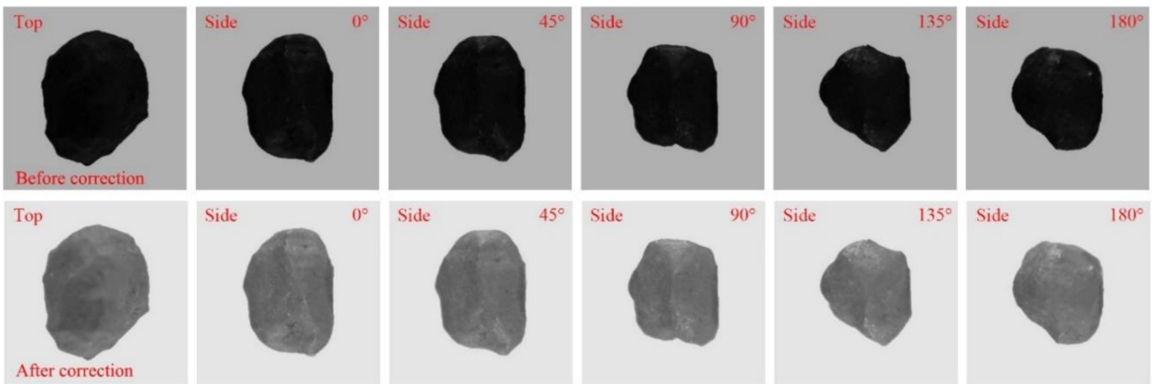

Figure 4. Gamma correction effect comparison.

2.3.3. Contour Extraction of Fertilizer Top and Side Images

During the image processing, the extraction of fertilizer contour is a key step, and its results directly affect the calculation accuracy of fertilizer shape characteristics in the later stage. In the top and side images of fertilizer after Gamma correction, fertilizer has strong boundary information. In edge detection, the selection of high and low threshold is very important, which directly determines the amount of edge information detected and the continuity of the edge. Since the high threshold controls the starting point of edge detection, the smaller the high threshold is, the more edge information will be retained, but the false edges will increase. On the contrary, if the high threshold is larger, although the false edges can be effectively suppressed, some edge information will also be lost. How to choose a suitable high and low threshold has an important influence on the selection of the correct edge point in the stage of edge detection and connection. Therefore, the edge detection algorithm based on the directional gradient is proposed to extract the contour of the fertilizer image accurately. The main steps are as follows:

(1) Suppose the high and low thresholds are h and l, respectively. After suppressing the non-maximum value of the gradient mode, the candidate edge points can be divided into three categories according to the range of the gradient mode: B_1, B_2, and B_3, which are defined as follows.

$$B_1=\{(x,y)\mid 0<|grad\, f(x,y)|<l\} \tag{10}$$

$$B_2=\{(x,y)\mid l\le|grad\, f(x,y)|\le h\} \tag{11}$$

$$B_3=\{(x,y)\mid |grad\, f(x,y)|\ge h\} \tag{12}$$

Where, B_1 is the set of non-edge pixels; B_2 is the set of possible edge pixels; B_3 is the set of edge pixels after non-maximum value suppression.

(2) Calculate the directional derivative of each pixel in the top and side image corrected with gamma, and calculate the gradient modulus based on the result of the directional derivative.

(3) Perform non-maximum suppression on the top and side image based on the gradient mode and determine the set of candidate edge points.

(4) Among the candidate edge points, the high and low thresholds are determined according to the minimization of the three types of gradient modulus variance. The high threshold is 102 and the low threshold is 44.

(5) Use recursive search for boundary point detection and edge connection and output image edges. The top and side contours of fertilizer are shown in Figure 5.

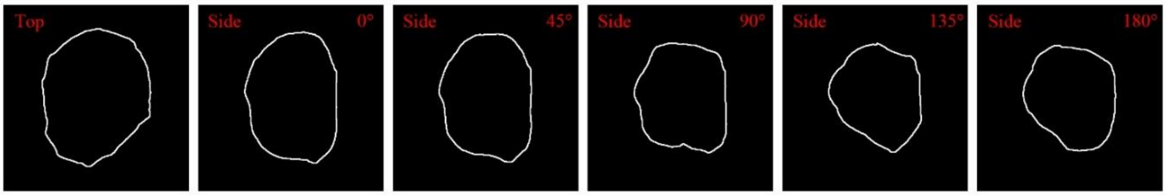

Figure 5. Top and side contour images of fertilizer.

2.3.4. Calculation of Fertilizer Particle Shape Parameters

In the top contour image, the parameters of fertilizer top contour perimeter L, area A, and the minimum circumscribed rectangle are obtained. The length of the minimum circumscribed rectangle represents the maximum size of the fertilizer in the top projection, and the width of the minimum circumscribed rectangle represents the maximum size perpendicular to the length direction. Therefore, the length and width of the minimum circumscribed rectangle are respectively equivalent to the length a_1 and width b_1 of the fertilizer, and then the fertilizer equiaxed ratio k_1 and roundness σ_1 are calculated according to formulas (1) and (3).

In the side contour image, the parameters of the minimum circumscribed rectangle are obtained. The width of the minimum circumscribed rectangle represents the line dimension of the fertilizer perpendicular to the length and width direction. To reduce the error, the average value of the minimum circumscribed rectangle width of all side contours is equivalent to the fertilizer thickness c_1, and then the fertilizer flake rate λ_1, sphericity φ_1, and granularity d_1 are calculated according to formulas (2), (6), and (7).

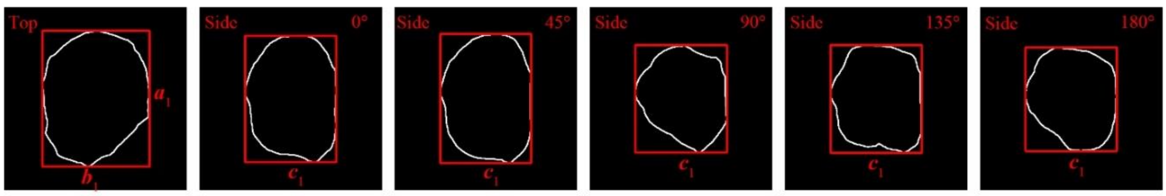

Figure 6. Fertilizer particle shape parameters.

3. Results and Discussion

3.1. Experiment Design

The three-dimensional scanning technology can transform various irregular, complex or non-standard target structure information into the data information, and then reconstruct the three-dimensional model of the target structure to achieve a precision measurement, which can replace the traditional measurement method [31]. To verify the measurement accuracy and speed of the fertilizer shape characteristic measuring instrument, a control experiment was designed. In the same order, the method proposed in the paper (FSI) and three-dimensional scanning method (TDS) were used to obtain the fertilizer shape characteristics.

In this study, the three-dimensional scanner produced by Beijing Xunheng Technology Co., Ltd. was used. The point cloud digital model of fertilizer was obtained by non-contact scanning, as shown in Figure 7. Three-dimensional scanner measuring the fertilizer shape characteristics were as follows:

(1) Obtain the point cloud digital model of fertilizer by three-dimensional scanning technology.

(2) Obtain the length a_2, width b_2, thickness c_2, area A_2, and perimeter L_2 of fertilizer by software.

(3) Calculate the equiaxed ratio k_2, flake ratio λ_2, roundness σ_2, and sphericity φ_2 of the fertilizer according to formula (1), (2), (3), and (6).

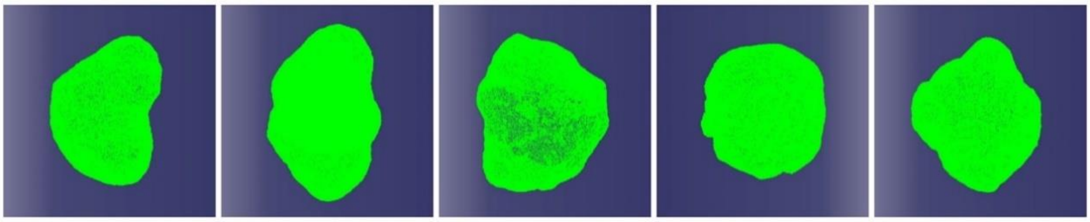

Figure 7. Three dimensional scanning of fertilizer.

According to the different material forms in fertilizers, fertilizers can be divided into the compound fertilizer (CF), the organic fertilizer (OF), and the biological fertilizer (BF). To test the applicability of the method proposed in this paper to different fertilizers, 100 compound fertilizers, 100 organic fertilizers, and 100 biological fertilizers produced by Shandong Guanxian Fufeng fertilizer Co., Ltd. were collected as experimental samples by random sampling [32]. Taking this sample as the research object, we measured the fertilizer shape characteristics. The distribution of each parameter was shown in Figure 8. To verify the accuracy of measurement, the experiment datas were summarized, processed, and analyzed.

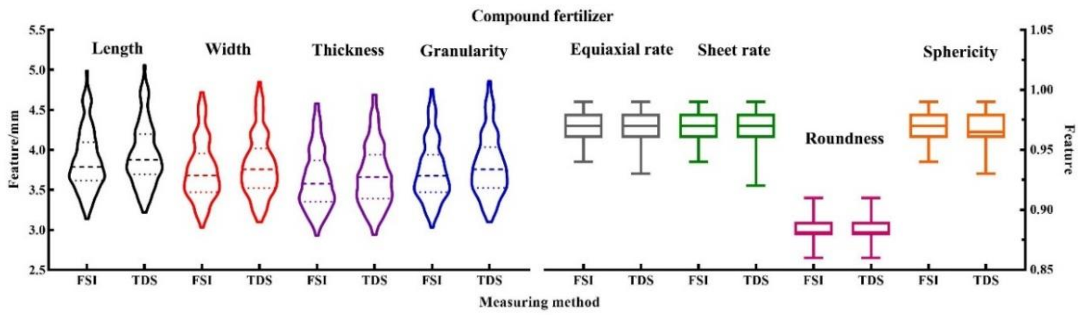

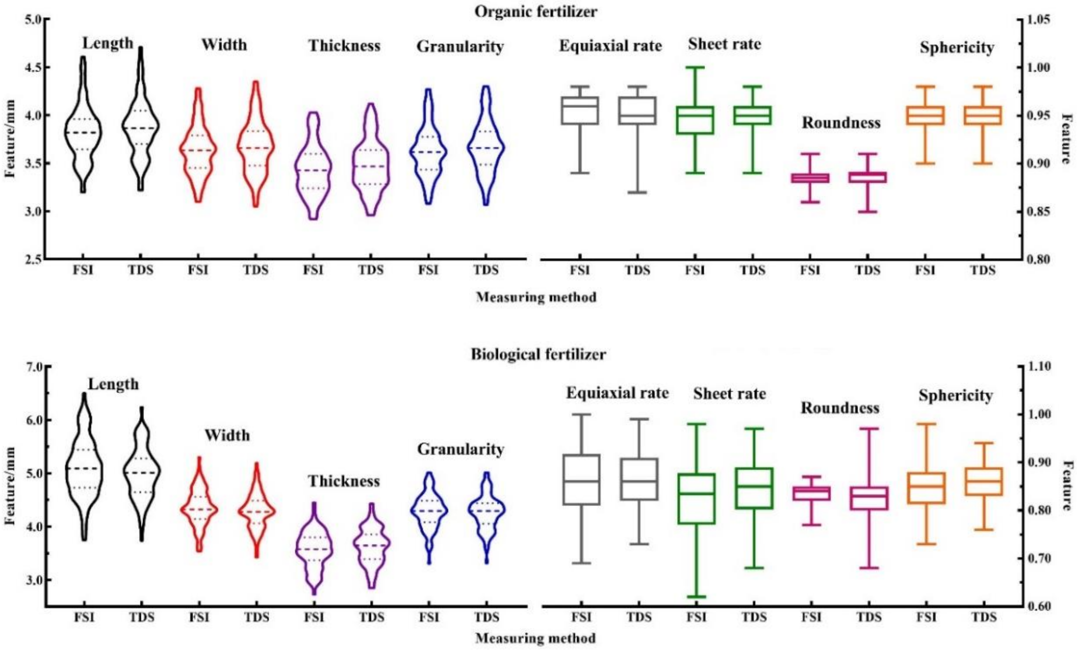

Figure 8. Distribution of fertilizer particle shape characteristic parameters.

It can be seen from Figure 8 that the length, width, thickness, and granularity of the fertilizers were all approximately normal distribution under different measurement methods, with a bell-shaped distribution of high in the middle and low at both ends. The length, width, thickness, median, upper quartile, lower quartile, and the peak value of probability density function distribution among the three fertilizers have small differences. Under different measuring methods, the differences of the mean value, the upper quartile and the lower quartile of the equiaxed rate, the flake rate, the roundness, and the sphericity of the three fertilizers were small. The results showed that the datas measured by the two methods are evenly distributed, with small fluctuation, high stability, and no significant difference.

3.2. Basic Statistical Processing

In order to further compare the measurement accuracy of the two measurement methods, the experiment datas were calculated statistically. The maximum value, minimum value, average value, range, and standard deviation of the fertilizer shape characteristics were calculated respectively, so as to prepare for the Grubbs test, *F* test, *t* test, and test analysis. The specific results were shown in Table 2. The average value and standard deviation respectively were:

$$\bar{x} = \frac{\sum_{i=1}^{n} x_i}{n} \tag{13}$$

$$S = \sqrt{\frac{\sum_{i=1}^{n}(x_i - \bar{x})^2}{n-1}} \tag{14}$$

Where, x_i is the sample value; n is the sample total number; $\bar{x}$ is the sample mean value; S is the sample standard deviation.

Table 2. Basic statistical results.

Project		a_1/a_2	b_1/b_2	c_1/c_2	k_1/k_2	λ_1/λ_2	σ_1/σ_2	φ_1/φ_2	d_1/d_2
	Maximum	4.99/5.06	4.72/4.85	4.58/4.69	0.99/0.99	0.99/0.99	0.91/0.91	0.99/0.99	4.76/4.86
CF	Minimum	3.14/3.22	3.03/3.10	2.93/2.94	0.94/0.93	0.94/0.92	0.86/0.86	0.94/0.93	3.03/3.10
	Average	3.86/3.94	3.74/3.81	3.62/3.67	0.97/0.97	0.97/0.96	0.89/0.88	0.97/0.97	3.74/3.80

	Standard deviation	0.38/0.39	0.38/0.39	0.38/0.39	0.01/0.01	0.01/0.02	0.01/0.01	0.01/0.01	0.38/0.39
OF	Maximum	4.61/4.71	4.28/4.35	4.03/4.12	0.98/0.98	1.00/0.98	0.91/0.91	0.98/0.98	4.27/4.30
	Minimum	3.20/3.22	3.10/3.05	2.92/2.96	0.89/0.87	0.89/0.89	0.86/0.85	0.90/0.90	3.08/3.07
	Average	3.82/3.87	3.63/3.67	3.43/3.48	0.95/0.95	0.94/0.95	0.88/0.89	0.95/0.95	3.62/3.67
	Standard deviation	0.28/0.30	0.26/0.28	0.26/0.27	0.02/0.03	0.02/0.02	0.01/0.01	0.02/0.02	0.26/0.27
BF	Maximum	6.50/6.24	5.30/5.19	4.45/4.43	1.00/0.99	0.98/0.97	0.87/0.97	0.98/0.94	5.01/5.01
	Minimum	3.75/3.74	3.54/3.43	2.73/2.85	0.69/0.73	0.62/0.68	0.77/0.68	0.73/0.76	3.31/3.32
	Average	5.10/5.00	4.36/4.29	3.57/3.63	0.86/0.86	0.83/0.85	0.84/0.83	0.85/0.86	4.29/4.26
	Standard deviation	0.54/0.47	0.34/0.32	0.34/0.34	0.08/0.06	0.07/0.07	0.04/0.05	0.05/0.04	0.32/0.32

3.3. Grubbs Test

In order to eliminate the abnormal data caused by negligent error, the Grubbs test is used in this study. The specific process is as follows:

(1) Rank the original test data from small to large, and obtain the average value and the standard deviation of the data.

(2) Calculate the statistic T_i according to formula (15), and the results are shown in Table 3.

(3) Compare the statistic T_i with the critical value $T_{\alpha,n}$ in the Grubbs test table (α is the significance level, n is the sample size). If $T_i \geq T_{\alpha,n}$, it means that x_i is a discrete value, which must be discarded, otherwise it should be reserved.

$$T_i = \frac{\bar{x}-x_i}{S} \quad (i=1, 2, 3, \ldots, 100) \tag{15}$$

Where, x_i is sample value; $\bar{x}$ is sample mean value; S is sample standard deviation.

Table 3. Grubbs test results.

T_i		*a*	*b*	*c*	*k*	*λ*	*σ*	*φ*	*d*
CF	FSI	2.92	2.58	2.55	2.56	1.92	3.13	2.46	2.69
	TDS	2.87	2.69	2.61	2.36	2.89	2.78	2.99	2.74
OF	FSI	2.80	2.51	2.29	2.62	2.83	2.94	2.62	2.49
	TDS	2.80	2.42	2.37	3.04	3.17	3.10	2.52	2.30
BF	FSI	2.58	2.82	2.61	2.22	2.87	1.81	2.73	3.06
	TDS	2.70	2.79	2.39	2.21	2.54	3.14	2.44	2.98

Query the Grubbs test value table, take $\alpha = 0.05$, $n = 100$, $T_{0.05,100} = 3.207$. Comparing the maximum value of each method in Table 3 with $T_{0.05,100}$, we find that each group of data is less than $T_{0.05,100}$. It shows that there is no discrete value in the original data of the group, and the data is effective and accurate.

3.4.F Test

The standard deviation can reflect the precision of a set of data. Different sets of data have different precision. F test is needed to test whether there is a significant difference between the two sets of data precision. To verify the data precision of the measurement methods, two evaluation methods were taken as one set, and the F test was carried out. The specific process is as follows:

(1) Calculate the value of F according to the formula (16), and the result is shown in Table 4.

$$F = \frac{{S_1}^2}{{S_2}^2} \quad ({S_1}^2 \geq {S_2}^2) \tag{16}$$

(2) Query the critical value in the F distribution table, take $\alpha = 0.05$, $n_1 = 100$, $n_2 = 100$, and the $F_{0.25\ (99,99)} = 1.76$ is obtained. If $F \le F_{0.25\ (99,99)}$, it means that there is no significant difference between the two sets of data precision, otherwise, there is a significant difference.

(3) Combined with the F value of each set of data in Table 4, it is found that each set of data is less than $F_{0.25\ (99,99)}$. Therefore, there was no significant difference in the measurement precision between the two sets of data.

Table 4. F test results.

***F* test**	***a***	***b***	***c***	***k***	***λ***	***σ***	***φ***	***d***
CF	1.03	1.05	1.08	1.60	1.10	1.02	1.53	1.05
OF	1.13	1.16	1.04	1.32	1.07	1.45	1.25	1.10
BF	1.37	1.09	1.00	1.56	1.25	1.65	1.52	1.02

3.5.T Test

To verify whether there is a significant difference between the mean values of the two sets of data, the t test is needed. Since the test datas of the two sets have same sample size, the t value is calculated according to formula (17), and the results are shown in Table 5.

$$t = |\bar{x}_1-\bar{x}_2| \sqrt{\frac{n}{S_1^2+S_2^2}} \tag{17}$$

Table 5. t test results.

***t* test**	***a***	***b***	***c***	***k***	***λ***	***σ***	***φ***	***d***
CF	1.38	1.13	0.97	1.61	0.96	0.99	1.67	1.16
OF	1.17	1.06	1.41	0.41	1.66	0.69	0.21	1.24
BF	1.38	1.37	1.14	0.19	1.91	1.93	1.59	0.56

Compare the calculated t value with $t_{\alpha,(n_1+n_2\text{-}2)}$ in the table of t distribution, if $t \le t_{\alpha,(n_1+n_2\text{-}2)}$, it indicates that there is no significant difference between the average values of the two groups of data. Taking α = 0.05, $t_{0.05,198}$ = 1.98 and combining the data in Table 5, it is found that the data of each group is less than $t_{0.05,198}$. Therefore, there is no significant difference between the average values of the data of each set.

3.6. Results Analysis

From the above results of the Grubbs test, F test, and t test, there is no significant difference between the test data of each set measured by the two measurement methods, indicating that both the two measurement methods can accurately measure the particle shape of fertilizer. The 3D scanning method needs more professional knowledge, and the post-processing time is longer. The instrument and method proposed in this paper can collect the top and side images of the fertilizer automatically, which can measure the fertilizer shape characteristics non-destructively, efficiently, accurately, and stably. So, it can replace the 3D scanning method to measure fertilizer shape characteristics.

4. Conclusions

In order to measure the fertilizers shape characteristics accurately, we propose a precision measuring instrument of fertilizer shape characteristics as well as its measuring method. The main conclusions of this paper are listed in the following:

(1) A measuring instrument and method of fertilizer shape characteristics are developed based on the binocular vision, which provided a theoretical basis for fertilizer production and quality inspection. The instrument adopts the intermittent static collection mode to collect the top and side images of the fertilizer at one time. The method adopts the edge detection algorithm based on the

directional gradient to extract the contour of the fertilizer image accurately.

(2) Fertilizer shape characteristics were measured by the three-dimensional scanning method and the method proposed in this paper. The test data were tested by the Grubbs test, *F* test, and *t* test. The results showed that $T<T_{0.05,100}$, $F<F_{0.025(99,99)}$, and $t<t_{0.05,198}$. It indicated that no significant difference was found between the measurement results, and the measuring instrument and method were accurate and reliable.

(3) The measuring test of three fertilizers has been completed by the instrument and method proposed in this paper. With the popularization of slow-release fertilizer and controlled-release fertilizer, and the increasingly variety of fertilizers, the other fertilizers types also need to be tested and verified.

Author Contributions: Conceptualization, H.Z. and J.W.; Methodology, H.Z. and S.L.; Validation, H.J.; Formal analysis, C.X.; Investigation, H.Z. and X.L.; Resources, J.W. and S.L.; Writing—original draft, H.Z.; Writing—review and editing, H.Z. and J.W.; Visualization, H.Z.; Supervision, H.Z. and J.W.

Funding: This research was funded by National Key Research and Development Plan of China, grant number 2016YFD0201104, National Apple Industry Technology System Project of China, grant number CARS-27 and Rice Industry Innovation Team of Modern Agricultural Technology System in Shandong Province.

Conflicts of Interest: The authors declare no conflict of interest.

References

1. Meloy, T. P. Fast fourier transforms applied to shape analysis of particle silhouettes to obtain morphological data. *Powder Technol.* **1977**, 17(1), 27-35.
2. Hyslip, J. P.; Vallejo, L. E. Fractal analysis of the roughness and size distribution of granular materials. *Eng. Geol.* **1997**, *48*(3), 231-44.
3. Blott, S. J.; Pye, K. Particle shape: a review and new methods of characterization and classification. *Sedimentology*. **2010**, *55*(1), 31-63.
4. Payan, M.; Khoshghalb, A.; Senetakis, K.; Khalili, N. Effect of particle shape and validity of G(max) models for sand: A critical review and a new expression. *Comput. Geotech.* **2016**, *72*, 28-41.
5. Vangla, P.; Roy, N.; Gali, M. L. Image based shape characterization of granular materials and its effect on kinematics of particle motion. *Granul. Matter.* **2018**, *20*(1), 6.
6. Altuhafi, F.; O'sullivan, C.; Cavarretta, I. Analysis of an image-based method to quantify the size and shape of sand particles. *J. Geotech. Geoenviron. Eng.* **2012**, 139(8), 1290–1307.
7. Cho, G. C.; Dodds, J.; Santamarina, J. C. Particle shape effects on packing density, stiffness, and strength: natural and crushed sands. *J. Geotech. Geoenviron. Eng.* **2006**, *133*(11), 591–602.
8. Wang, W.; Coop, M. R. An investigation of breakage behaviour of single sand particles using a high-speed microscope camera. *Géotechnique.* **2016**, *66*(12), 984–998.
9. Zhao, B.; Wang, J.; Coop, M. R.; Viggiani, G.; Jiang, M. An investigation of single sand particle fracture using X-ray micro-tomography. *Géotechnique.* **2015**, *65*(8), 625–641.
10. Antony, S. J.; Kuhn, M. R. Influence of particle shape on granular contact signatures and shear strength: new insights from simulations. *Int. J. Solids Struct.* **2004**, *41*(21), 5863–5870.
11. Cleary, P. W.; Sawley, M. L. DEM modelling of industrial granular flows: 3D case studies and the effect of particle shape on hopper discharge. *Appl. Math. Model.* **2002**, *26*(2), 89–111.
12. Haider, A.; Levenspiel, O. Drag coefficient and terminal velocity of spherical and non-spherical particles. *Powder Technol.* **1989**, *58*(1), 63–70.
13. Xia, W. Role of particle shape in the floatability of mineral particle: an overview of recent advances. *Powder Technol.* **2017**, *317*, 104–116.
14. Xu, L. Z.; LI, Y.; LI, Y. M.; Chai X. M.; Qiu, J. Research progress on cleaning technology and device of grain combine harvester. *Trans. Chin. Soc. Agric. Mach.* **2019**, *50*(10), 1-16.
15. Hou, H. M.; Cui, Q. L.; Guo, Y. M. Effects of moisture contents of threshed materials from whole-feeding combine for foxtail millet on their suspension characteristics. *Trans. Chin. Soc. Agric. Eng.* **2018**, *34*(24), 29-35.
16. Kan, H. F.; Su, J. L.; Tang, C. J. Anti-caking measure for compound fertilizer by acid ammoniation process and its application. *Phosphate Compd. Fert.* **2016**, *31*(06), 31-32.

17. Silverberg, J.; Lehr, J. R.; Hoffmeister, G. Fertilizer caking, microscopic study of the mechanism of caking and its prevention in some granular fertilizers. *J. Agric. Food Chem.* **1958**, *6*(6), 442-448.
18. Basu, S.; Kumar, N. Mathematical model and computersimulation for release of nutrients from coatedfertilizer granules. *Math. Comput. Simul.* **2008**, *79*, 634-646.
19. Fernlund, J. M. R. Image analysis method for determining 3-D shape of coarse aggregate. *Cem. Concr. Res.* **2005**, *35*(8), 1629-1637.
20. Zhang, D.; Huang, X. M.; Zhao, Y. L. Investigation of the shape, size, angularity and surface texture properties of coarse aggregates. *Constr. Build. Mater.* **2012**, *34*(g), 330-336.
21. Mora, C. F.; Kwan, A. K. H. Sphericity, shape factor, and convexity measurement of coarse aggregate for concrete using digital image processing. *Cem. Concr. Res.* **2000**, *30*(3), 351-358.
22. Liu, Q. B.; Xiang, W.; Budhu, M.; Cui, D. S. Study of particle shape quantification and effect on mechanical property of sand. *Rock Soil Mech.* **2011**, *32*(S1), 190-197.
23. Zhang, J. F.; Ye, J. B.; Chen, J. S.; Li, S. L. A preliminary study of measurement and evaluation of break-stone grain shape. *Rock Soil Mech.* **2016**, *37*(2), 343-349.
24. Xiao, B. L.; Yang, Z.Q.; Chen, D. X.; Gao, Q. Evaluation of the quantifying methods for shape characteristics of filling aggregate. *J. Tianjin Univ.* **2019**, *52*(5), 545-553.
25. LI, B. X.; Wang, W.; Chen, M. Y.; Ye, M. Isometric ratio, roundness and sphericity of coarse aggregates and their relationship. *J. Build. Mater.* **2015**, *18*(04), 531-536.
26. Kuo, C. Y.; Freeman, R. B. Imaging indices for quantification of shape, angularity, and surface texture of aggregates. *J. Transp. Res. Board.* **2000**, *1721*(1), 57－65.
27. Wadell, H. Volume, shape, and roundness of rock particles. *J. Geol.* **1932**, *40*, 443－451.
28. Krumbein, W. C. Measure and geological significance of shape and roundness of sedimentary particles. *J. Sediment. Petrol.* **1941**, *1*(11), 64-72.
29. Masad, E.; Olcott, D.; White, T.; Tashman, L. Correlation of fine aggregate imaging shape indices with asphalt mixture performance. *J. Transp. Res. Board.* **2001**, *1757*(1), 148-156.
30. Xi, R.; Hou, J. L.; Li, L. C. Fast segmentation on potato buds with chaos optimization-based K-means algorithm. *Trans. Chin. Soc. Agric. Eng.* **2019**, *35*(05), 190-196.
31. Yang, B. S.; Liang, F. X.; Huang, R. G. Progress, challenges and perspectives of 3D LiDAR point cloud processing. *Acta Geodaetica et Cartographica Sinica.* **2017**, *46*(10), 1509-1516.
32. Yuan, J.; Liu, Q. H.; Liu, X. M.; Zhang, T.; Zhang, X. H. Granular Multi-flows fertilization process simulation and Tube structure optimization in nutrient proportion of variable rate fertilization. *Trans. Chin. Soc. Agric. Mach.* **2014**, *45*(06), 125-132.